Projectile mass dependence for the interaction of copper with ^{14}N, ^{16}O, and ^{22}Ne at ~540 MeV total projectile kinetic energy

J. P. Whitfield* and N. T. Porile

Department of Chemistry, Purdue University, West Lafayette, Indiana 47907
(Received 19 May 1994)

Using thick-target, thick-catcher recoil range techniques, target residues from the interaction of copper with 40 MeV/nucleon ^{14}N, 35 MeV/nucleon ^{16}O, and 25 MeV/nucleon ^{22}Ne have been studied. Isobaric and mass yield distributions as well as longitudinal momentum transfer information have been determined from measured cross section, average forward range, and forward-to-backward ratios. Comparisons with previously reported reactions involving copper and lighter ions have been made. Comparisons of the data with the interaction-evaporation model Boltzmann-Uehling-Uhlenbeck-PACE are presented.

PACS number(s): 25.70.Mn

I. INTRODUCTION

As beam energies increase from 10 MeV/nucleon to 100 MeV/nucleon the mean field between the interacting systems becomes decreasingly important, while two-body nucleon-nucleon interactions begin to dominate the reaction mechanism. This transition leads to a wide variety of interesting phenomena which appear at intermediate energies, such as a transition from complete to incomplete fusion [1,2], preequilibrium emission [3,4], saturation of momentum transfer [5–12], energy deposition [11,12], etc. This evolution in reaction dynamics with projectile energy per nucleon has been well studied over the past ten years for a wide variety of projectile-target combinations [13–21]. In this work we examine the effect of the variation in projectile mass at a given total projectile kinetic energy on the reaction dynamics.

Utilizing thick-target, thick-catcher recoil range techniques interactions between Cu and 25 MeV/nucleon ^{22}Ne, 35 MeV/nucleon ^{16}O, and 40 MeV/nucleon ^{14}N have been measured and compared with previously reported 45 MeV/nucleon ^{12}C [14] and 90 MeV/nucleon ^{6}Li [15]. All these reactions involve nearly the same total projectile kinetic energy of ~540 MeV. With increasing projectile mass it has been reported that there is decreasing incomplete fusion due to greater thermalization of the energy during the initial interaction [22]. However, Leray has summarized results which appear to be contrary to these findings [23]. Thus, the projectile mass dependence has been further explored to examine the effect on the mean linear momentum transferred ($\langle LMT \rangle$)

from projectile to target during the initial interaction and, in turn, on incomplete fusion of the projectile-target system. We also report here results from the comparison of the reaction observables with Boltzmann-Uehling-Uhlenbeck (BUU)-PACE [24–29] simulation results.

II. EXPERIMENTAL DETAILS

Interactions between Cu and 25 MeV/nucleon ^{22}Ne, 35 MeV/nucleon ^{16}O, and 40 MeV/nucleon ^{14}N were performed at the National Superconducting Cyclotron Laboratory (NSCL). Beam intensity measurements were performed using a calibrated Faraday cup and recorded using a current integrator. The intensities ranged from 1.4×10^{10} ions/s for ^{14}N to 3.8×10^{11} ions/s for ^{16}O. Similar target stacks were used for each of these experiments. For the ^{16}O and ^{22}Ne reactions these consisted of a 20.1 mg/cm^2 target Cu foil surrounded by four 10.1 mg/cm^2 carbon catcher foils (nearest the target) and guard foils. For the ^{14}N reaction, a 20.7 mg/cm^2 Cu foil was surrounded by 10.1 mg/cm^2 Mylar catcher and guard foils. Catcher foils serve to collect products recoiling out of the target in the forward or backward directions. Guard foils were utilized to measure direct activation of impurities in the carbon or Mylar catcher foils. Beam energies at the center of the target were reduced to 500 MeV for the ^{22}Ne reaction, 544 MeV for the ^{16}O reaction, and 540 MeV for the ^{14}N reaction due to energy loss in the various foils [30].

Two irradiations were performed for each experiment, one of short duration (15 min–1 h) and the other of longer duration (3–6 h). Following irradiation the foils from the target stacks were separated and assayed utilizing calibrated intrinsic Ge and Ge(Li) γ-ray spectrometers. For the short irradiations analysis of the foils was performed at NSCL and began ~30 min after the end of bombardment (EOB) and typically continued for 24 h. For the long irradiations the samples were returned to Purdue where counting began ~1 d after EOB and continued for

---

*Present address: Department of Chemistry, Carnegie Mellon University, Pittsburgh, PA 15213.

several months. The code SAMPO [31] was utilized to determine γ-ray intensities. Decay curves were constructed from these intensities and analyzed using the code CLSQ [32]. Nuclidic assignments were made upon comparison with tabulated nuclidic γ-ray energies and half-lives [33].

III. RESULTS

The production cross sections for the individual products are listed in Table I. Cross sections were obtained

by summing the measured activity from the target and catcher foils. For products where multiple γ rays were detected the values are weighted averages over the set of these γ rays. The uncertainties are the larger of the standard deviations in the mean value for the set of γ rays for a given product and the estimated uncertainty of the individual determination of these γ rays. Nuclides where only a single determination of a single γ ray was made had an additional 10% uncertainty folded in.

As mentioned above, guard foils were included in the target stack so that corrections due to direct production of impurities in the carbon or Mylar foils could be made. ^{22}Na and ^{24}Na required a reduction of 23% and 10%, respectively, for the ^{16}O reaction, and 5–6% reductions for the other projectiles. None of the heavier products required a correction larger than 1% due to catcher foil activation. The listed products labeled C^+ include contributions from proton-rich progenitors and C^- denotes those with contributions from neutron-rich progenitors. Those labeled I, independent, have no progenitor contribution.

The recoil results are listed in Table II, expressed in terms of the average forward range FW and forward-to-backward ratio F/B. Here, W is the target thickness in mg/cm^2 and F and B are the fraction of total activity collected in the forward and backward catchers, respectively. Again, due to direct activation of impurities in the catchers, corrections must be made to these FW and F/B values. Only the FW values for the sodium nuclides

TABLE I. Production cross sections for the interaction of copper with ~540 MeV ^{22}Ne, ^{16}O, and ^{14}N ions.

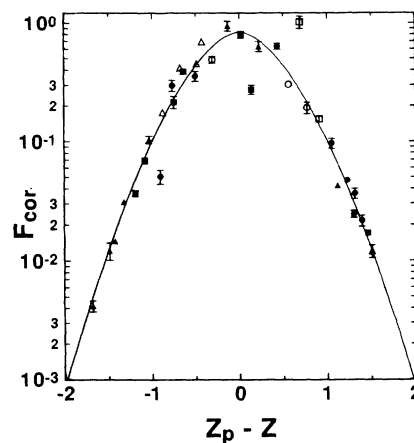| Nuclide	Type	^{22}Ne σ (mb)	^{16}O σ (mb)	^{14}N σ (mb)
^{22}Na	C^+	0.18±0.05	2.86±0.26	2.56±0.88
^{24}Na	C^-	4.60±0.35	4.07±0.25	3.59±0.37
^{28}Mg	C^-	0.41±0.12	0.30±0.03	0.27±0.04
^{34}Cl^m	C^+	0.59±0.08	0.62±0.09	0.60±0.08
^{39}Cl	C^-	0.53±0.04	0.47±0.06	0.41±0.06
^{41}Ar	C^-	1.18±0.02	1.01±0.10	0.89±0.09
^{42}K	I	6.82±0.76	6.14±0.70	7.49±0.81
^{43}K	C^-	2.06±0.04	1.70±0.02	1.97±0.12
^{43}Sc	C^+		11.0±1.18	
^{44}Sc	I	4.02±0.43	6.97±0.82	5.19±0.54
^{44}Sc^m	I	10.8±1.1	14.0±1.1	20.0±1.6
^{46}Sc	I	16.9±1.8	17.0±0.03	18.6±0.9
^{47}Ca	C^-	0.12±0.01		
^{47}Sc	I		6.01±0.59	7.56±0.76
^{48}Sc	I	1.12±0.50	0.82±0.10	0.66±0.19
^{48}V	I	27.2±2.5	32.8±0.6	36.6±2.7
^{48}Cr	C^+	0.20±0.02	0.84±0.07	0.91±0.05
^{49}Cr	C^+	4.74±3.46	8.28±0.60	7.22±0.77
^{51}Cr	C^+	90.9±10.0	99.3±9.7	96.0±9.7
^{52}Mn	C^+	27.7±1.2	27.8±0.9	32.9±2.0
^{52}Mn^m	I		3.76±0.38	3.71±0.41
^{52}Fe	C^+	0.19±0.03	0.47±0.05	0.59±0.07
^{54}Mn	I	90.2±9.7	74.7±7.3	73.4±7.5
^{55}Co	C^+	2.66±0.55	4.39±0.11	4.27±0.29
^{56}Mn	C^-	9.64±0.28	6.13±0.13	7.44±0.53
^{56}Co	I	21.2±0.9	23.7±0.06	25.0±1.4
^{56}Ni	C^+	0.08±0.01	0.15±0.03	
^{57}Co	I	104±10	84.6±3.1	81.4±4.2
^{57}Ni	C^+	1.65±0.06	2.37±0.0	2.48±0.16
^{58}Co	I	127±9	93.1±6.2	91.4±5.4
^{59}Fe	C^-	5.18±0.42	2.97±0.0	2.72±0.40
^{60}Co	I	8.97±0.64	20.2±1.1	20.4±4.4
^{60}Cu	C^+	5.40±0.57	9.92±0.50	9.35±0.67
^{61}Co	C^-			3.23±0.18
^{61}Cu	C^+	48.8±3.5	43.3±2.1	40.8±3.6
^{62}Zn	C^+	3.92±1.07	5.05±0.30	4.68±0.58
^{63}Zn	C^+	27.6±0.5	20.4±2.4	15.5±2.0
^{64}Cu	I	100±12	77.5±9.5	
^{65}Ni	C^-	0.85±0.11	0.45±0.11	
^{65}Zn	C^+	47.5±7.0	25.7±2.3	19.8±2.0
^{66}Ni	C^-	11.3±1.5		
^{66}Ga	C^+	7.63±2.53		
^{67}Ga	C^+	9.42±0.14		
^{69}Ge	C^+	1.52±0.78		

FIG. 1. Fractional isobaric yield distribution for the interaction of Cu with 35 MeV/nucleon ^{16}O ions. The curve represents the fitted values from Eqs. (1) and (2) at A=51. Symbols indicate the products mass region: (●) A =22–46, (solid triangle) A=47–57, and (solid square) A=58–65. Open symbols represent independent yields and solid symbols represent corrected cumulative yields. The data have been scaled to A=51.

required correction, the reduction amounting to $\sim 5\%$ for all targets. Owing to the large corrections to the activity of the backward catcher, the F/B values had to be increased by as much as 700%. Although these corrections are extremely large, F/B was used only for qualitative information so that the uncertainties introduced by this procedure are inconsequential.

IV. DISCUSSION

A. Isobaric yield distribution

A ten-parameter modified version [34] of Rudstam's [35] equation has been utilized to estimate the cross section of those products undetectable by our experimental methods:

$$\alpha(Z.A) = \exp[\alpha_1 + \alpha_2 A + \alpha_3 A^2 + \alpha_4 A^3 + (\alpha_5 + \alpha_6 A + \alpha_7 A^2)|Z_p - Z|^{\alpha_8}], \tag{1}$$

$$Z_p = \alpha_9 A + \alpha_{10} A^2. \tag{2}$$

TABLE II. Recoil properties for the interaction of copper with ~ 540 MeV ^{22}Ne, ^{16}O, and ^{14}N ions.

Nuclide	^{22}Ne		^{16}O		^{14}N	
	FW (mg/cm^2)	F/B	FW (mg/cm^2)	F/B	FW (mg/cm^2)	F/B
^{22}Na	14.2±1.8		7.46±1.40		7.07±0.75	
^{24}Na	11.6±1.7		7.18±0.07		5.73±0.60	
^{28}Mg	8.14±0.12		4.54±0.86		4.38±0.49	
^{34}Cl^m	5.32±1.58		3.90±0.93		3.74±0.63	
^{39}Cl	3.95±0.62		3.39±0.45			
^{41}Ar	4.35±0.54		2.88±0.47			
^{42}K	4.35±0.51		3.21±0.54		2.57±0.47	
^{43}K	4.20±0.06	124±17	3.13±0.11	308±66	2.10±0.23	
^{43}Sc			2.63±0.42	41.7±9.6		
^{44}Sc	2.67±0.36	53±4	1.91±0.06	25.5±5.0	2.52±0.27	
^{44}Sc^m	4.18±0.08	91±16	4.68±0.95		2.66±0.27	441±58
^{46}Sc	3.77±0.42	91±11	2.80±0.03	570±250	2.28±0.23	140±28
^{47}Ca	3.98±0.59					
^{47}Sc			2.92±0.43	349±205	2.30±0.23	241±43
^{48}Sc	4.01±0.39	99±28	3.06±0.46		1.95±0.75	
^{48}V	3.74±0.04		2.76±0.05		2.28±0.23	358±88
^{48}Cr	3.68±0.09	486±93	2.87±0.01		2.17±0.23	213±57
^{49}Cr	3.54±0.12	61±12	2.50±0.19	56.6±15.6	2.61±0.33	
^{51}Cr	3.41±0.40		2.58±0.38		2.01±0.20	406±135
^{52}Mn	3.56±0.03	136±9	2.71±0.06		2.12±0.21	
^{52}Fe	3.98±1.08		2.77±0.46		2.32±0.24	
^{54}Mn	3.33±0.38		2.34±0.35		1.66±0.23	
^{55}Co	3.38±0.12		2.06±0.98		1.57±0.19	
^{56}Mn	3.13±0.19		2.04±0.20		1.74±0.24	
^{56}Co	2.99±0.03	160±13	2.06±0.40		1.54±0.15	
^{56}Ni			1.83±0.55			
^{57}Co	2.82±0.13	259±15	1.73±0.07	45.3±12.0	1.33±0.13	171±26
^{57}Ni	2.99±0.05	55±14	2.12±0.21		1.45±0.15	
^{58}Co	2.71±0.03		1.85±0.13	280±43	1.17±0.14	169±36
^{59}Fe	1.97±0.10		1.19±0.07		0.94±0.10	
^{60}Co	1.73±0.22		1.28±0.09		1.07±0.14	
^{60}Cu	2.59±0.40		1.29±0.10			
^{61}Co					0.54±0.06	23±5
^{61}Cu	2.21±0.06	178±10	0.99±0.06	50.6±14.9	0.74±0.08	
^{62}Zn	2.68±0.22		1.41±0.17		0.78±0.08	
^{63}Zn	2.29±0.11					
^{65}Zn	2.42±0.27		0.78±0.12		0.61±0.07	
^{66}Ni	3.59±0.50					
^{66}Ga	3.97±0.46					
^{67}Ga	4.36±0.01	104±28				
^{69}Ge	5.92±0.43					

TABLE III. Parameters utilized in the fit of Eqs. (1) and (2) to experimental cross sections.

Parameter	^{22}Ne	^{16}O	^{14}N
α_1	11.43 ± 1.09	10.06 ± 0.74	16.89 ± 0.25
α_2	-1.01 ± 0.09	-0.83 ± 0.06	-1.38 ± 0.02
α_3	$(2.80\pm0.21)\times10^{-2}$	$(2.45\pm0.14)\times10^{-2}$	$(3.79\pm0.05)\times10^{-2}$
α_4	$-(2.18\pm0.16)\times10^{-4}$	$-(2.03\pm0.11)\times10^{-4}$	$-(3.10\pm0.04)\times10^{-4}$
α_5	3.85 ± 0.76	1.27 ± 0.33	-0.48 ± 0.11
α_6	-0.22 ± 0.03	-0.15 ± 0.01	$-(7.1\pm0.5)\times10^{-2}$
α_7	$(1.97\pm0.28)\times10^{-3}$	$(1.60\pm0.15)\times10^{-3}$	$(8.58\pm0.54)\times10^{-4}$
α_8	1.63 ± 0.03	1.70 ± 0.04	1.89 ± 0.01
α_9	0.47 ± 0.00	0.48 ± 0.00	0.48 ± 0.00
α_{10}	$-(1.47\pm0.12)\times10^{-4}$	$-(3.12\pm0.10)\times10^{-4}$	$-(2.10\pm0.03)\times10^{-4}$

Details of the procedure used to obtain the various constants in the above equation have been presented previously [13–16]. The values obtained for α_1–α_{10} for these reactions are given in Table III.

We have shown previously that the isobaric yields are approximately invariant over the intermediate energy range for reactions of Cu independent of projectile mass [15]. As an example of the present results, Fig. 1 shows the isobaric yield distribution for the ^{16}O reaction scaled to $A = 51$. The results show that the parametrization produces a good fit to data. Both the ^{14}N and ^{22}Ne reactions produced similar fits, where the mean deviation of the products from the curve was ~ 20–$25\,\%$.

B. Mass yield distribution

By combining the calculated cross sections of the unmeasured nuclides from Eq. (1) with experimental cross sections, we can obtain an estimate of the total cross section at each mass number. A 20–25% uncertainty is assumed for the calculated cross sections on the basis of the agreement of measured yields with Eq. (1). The mass yield distributions are presented in Fig. 2.

Comparing the ^{14}N and ^{16}O projectiles with previously reported 45 MeV/nucleon ^{12}C [14], we find that between 35 and 45 MeV/nucleon the mass yield distribution remains nearly unchanged for ^{12}C to ^{16}O projectiles. The distribution shows a maximum at $A \sim 55$, decreases exponentially for lighter products to $A \sim 25$, and then increases for the lightest products. It appears that as the mass of the projectile increases the minimum in the distribution becomes more shallow. This may be an indication of increasing fragmentation processes with increasing projectile mass.

Although the general trend of the ^{22}Ne distribution is similar, it appears to peak at a larger mass, $A \sim 60$. This may be a result of the increasing likelihood of fusion with decreasing projectile energy per nucleon. It has been shown that for the interaction of copper with ^{12}C [14] and ^{20}Ne ions [17] the maximum momentum transferred from the projectile to the target peaks at ~ 25 MeV/nucleon. The shift in the mass yield distribution to larger masses for the ^{22}Ne reaction may be a result of this effect, assuming an increase in momentum transferred directly relates to an increase in mass transfer. We

have shown previously that with increasing projectile energy for ^{12}C + Cu the peak in the mass yield distribution moves toward lower masses [14]. The present data along with the 45 MeV/nucleon ^{12}C + Cu results are compared with the curve representing this trend in Fig. 3. From this comparison it appears that the shift in the peak of

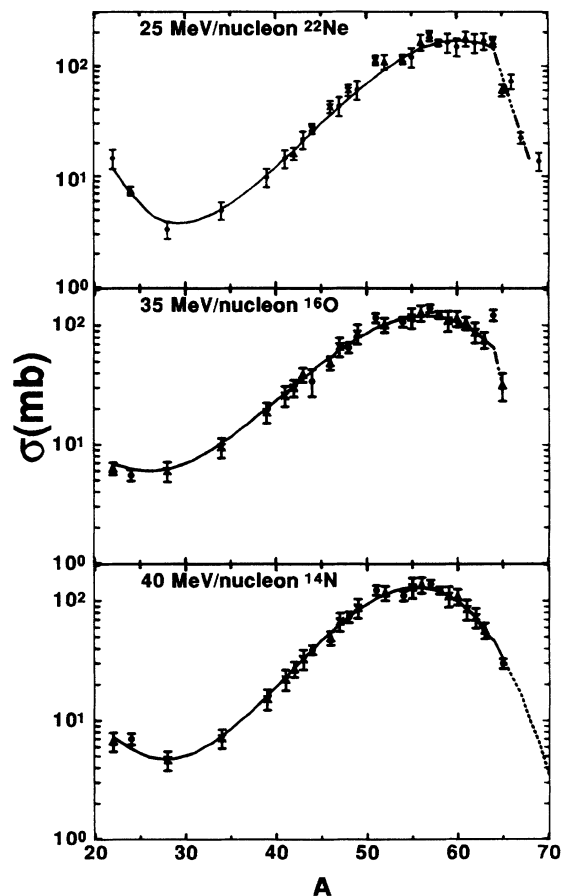FIG. 2. Mass yield distribution for the interaction of Cu with 25 MeV/nucleon ^{22}Ne, 35 MeV/nucleon ^{16}O, and 40 MeV/nucleon ^{14}N. The curve represents the distribution calculated from Eqs. (1) and (2). The points are experimental yields corrected for unmeasured products at a given A. The different symbols reflect the fractional contribution of the experimental cross sections to a given isobar: ($\bullet$) $> 50\%$, ($\triangle$) 20–50%, and ($\star$) $< 20\%$. The dashed and dot-dashed lines are an extrapolation for $A > 64$.
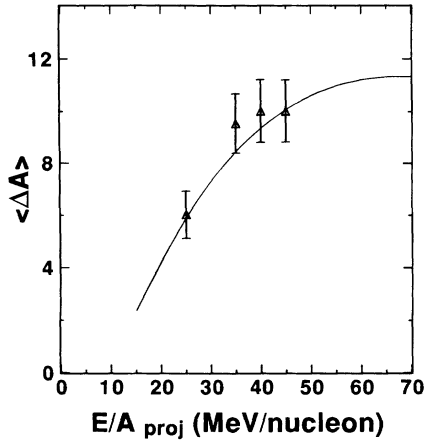
FIG. 3. Comparison of energy dependence of mean mass loss from the target (ΔA) for the interaction of copper with 25 MeV/nucleon ^{22}Ne, 35 MeV/nucleon ^{16}O, 40 MeV/nucleon ^{14}N, and 45 MeV/nucleon ^{12}C [14] with a fit obtained from 15 to 90 MeV/nucleon ^{12}C + Cu data [16].

the mass yield is clearly an effect of the projectile energy per nucleon.

C. Fractional velocity transfer

The velocity of the residual nucleus along the beam direction $v_{\parallel}$ and in turn the mean longitudinal momentum transfer $\langle$LMT$\rangle$ can be obtained from the recoil range FW using a previously described procedure [13–16]. It has been shown by Winsberg and Alexander [36] that the velocity corresponding to FW is just $v_{\parallel}$ for large LMT. Since large LMT is signified by large F/B values, this approach is applicable to the present data. We have used the code TRIM [30] to obtain the range-energy tables used in this analysis.

It is known that a significant change in production cross section along the depth of the target can affect the conversion from FW to $v_{\parallel}$ [37]. We have shown previously [15] that reactions induced by ^{12}C ions above 35 MeV/nucleon required no correction for this effect. Thus, since the projectile masses of ^{16}O and ^{14}N are close to ^{12}C and the projectile energies lie at or above this energy, we assume these reactions also require no correction. On the other hand, at 25 MeV/nucleon corrections for several products from the ^{12}C + Cu reaction were necessary. Therefore we felt it necessary to examine the ^{22}Ne reaction for this effect. Excitation functions were constructed from the Pieńkowski et al. [17] data for 8–48 MeV/nucleon ^{20}Ne + Cu. We used a formula developed by Hazan and Blann [37],

$$R = FW[(s_u + s_d)/2s_d] , \qquad (3)$$

where s_u and s_d are the cross sections at the upstream and downstream faces of the target, respectively. We have applied a correction to those data where the difference between s_u and s_d exceeded 50% of the uncertainty

associated with the experimental cross sections. Seven products ranging from ^{43}K to ^{52}Mn required corrections of 4–10%, while the largest corrections were required for the trans-target products, where corrections ranged from $\sim 10\%$–15%.

The $v_{\parallel}$ values obtained from the recoil data as discussed above are conveniently presented in terms of the velocity of the presumed compound nucleus v_{CN}. The resulting fractional velocity transfers $v_{\parallel}/v_{CN}$ are shown in Fig. 4 as a function of mass loss from the target, ΔA.

The $v_{\parallel}/v_{CN}$ values for the interaction of copper with 35 MeV/nucleon ^{16}O and 40 MeV/nucleon ^{14}N display a similar dependence on ΔA, with near-target products exhibiting very low values that increase to a plateau or maximum for the lightest products. This trend is similar to that previously reported for ^{12}C ions of comparable energy [13,14]. Although the ^{22}Ne + Cu distribution shows a similar behavior for products lower in mass than the target, there is increasing fractional velocity transfer with increasing product mass for the trans-target products. This signifies that these products are produced by a mechanism involving increasingly complete fusion with increasing mass, although a compound nucleus does not
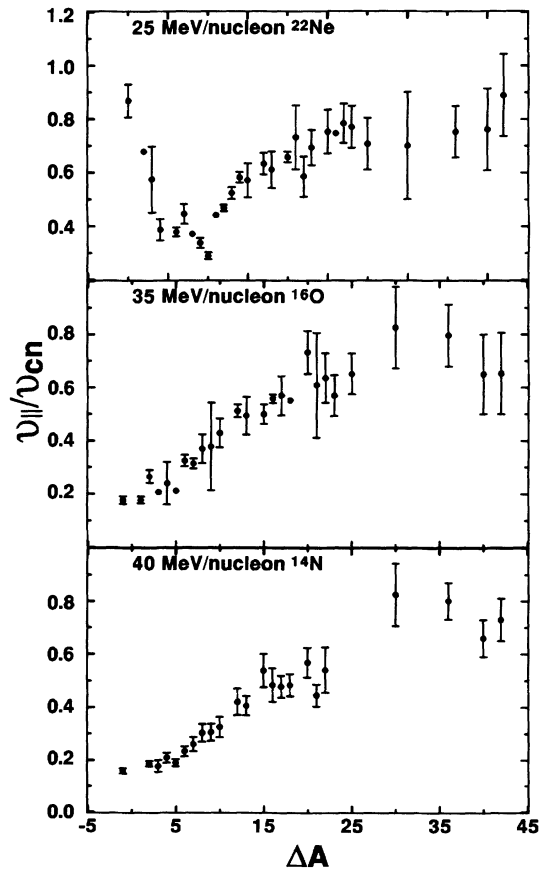

FIG. 4. Fractional velocity transfer for the interaction of Cu with 25 MeV/nucleon ^{22}Ne, 35 MeV/nucleon ^{16}O, and 40 MeV/nucleon ^{14}N.

appear to be formed. Pieńkowski *et al.* [17] have explained this V-shaped distribution centered about the target mass as resulting from the varying contribution of inelastic or few-nucleon transfer processes and full momentum transfer to the near-target products.

The absence of these trans-target products at larger fractional velocity transfer for the reactions at energies >25 MeV/nucleon studied here indicates the decreasing importance of fusion-type mechanisms in the initial stages of the interaction at higher projectile energy per nucleon. Similar results for trans-target products have been found for the interaction of copper with ^{12}C at 15 and 22 MeV/nucleon [14,21] and 8–28 MeV/nucleon ^{20}Ne [17].

D. Linear momentum transfer

The mean longitudinal momentum transfer $\langle P_\parallel \rangle$ is obtained by estimating the average mass of the prefragment leading to a given residual nucleus of longitudinal velocity

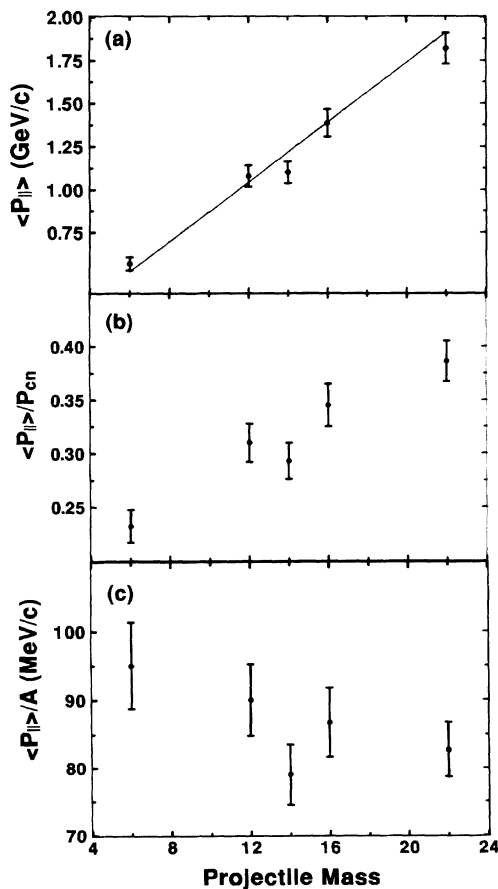
FIG. 5. Variation with projectle mass of (a) mean momentum transfer, (b) fractional momentum transfer, and (c) LMT per incident nucleon at a total projectile kinetic energy of ~540 MeV. The solid line in (a) shows the dependence of the reciprocal of projectile energy per nucleon normalized to the LMT at oxygen.

$v_\parallel$, as described in previous publications from our group [13–16]. The product of this prefragment mass and $v_\parallel$ is then $P_\parallel$ for the given product. By weighting each $P_\parallel$ by its given production cross section we obtain $\langle P_\parallel \rangle$, the mean LMT. Figure 5 displays various aspects of the variation of mean LMT with projectile mass. Minor adjustments using our previous results for 15–90 MeV/nucleon ^{12}C interactions with copper [13–15] have been made for the slight differences in bombarding energy. Thus, the values displayed in Fig. 5 are for a constant total projectile energy of 540 MeV.

It is apparent that the mean LMT increases with projectile mass. This trend appears to be a consequence of the decreasing energy per nucleon E/A with increasing mass at constant total projectile energy and the known fact that the maximum LMT in the reactions of present interest occurs at ~25 MeV/nucleon [14,15]. The correlation with E/A can be seen by the agreement of the solid line with the data. This line shows the increase with mass of the reciprocal of E/A.

The fractional momentum transfer, depicted in Fig. 5(b), also increases with mass, but to a lesser extent than the LMT. It appears as if the lighter projectiles can transfer momentum more efficiently than the heavier ones. This trend is shown more transparently in Fig. 5(c), where it is noted that the momentum transfer per incident nucleon decreases with projectile mass.

E. Comparison with calculations

Since mean field effects as well as nucleon-nucleon collisions play a role in the reaction dynamics at energies of present interest, calculations have been performed using the Boltzmann-Uehling-Uhlenbeck (BUU) [24–28] transport equation to simulate the ^{22}Ne and ^{16}O reactions. The calculation has been coupled with the deexcitation code PACE [29] in order to produce reaction products along with their kinematic properties.

A more detailed explanation of the procedure employed in the simulation has been given elsewhere [15]. Briefly, each nucleon in the projectile-target system is represented by 100 test particles in BUU. A complete simulation consisted of running 100 individual simulations over a range of impact parameters which correspond to the geometric cross section for that interval. The calculation follows each test particle through six-dimensional phase space to a stopping time of 120 fm/c for the ^{16}O reaction and 150 fm/c for the ^{22}Ne reaction.

The nuclear mean field is estimated using a Skyrme parametrization:

$$U = a\left(\frac{\rho}{\rho_0}\right) + b\left(\frac{\rho}{\rho_0}\right)^\sigma, \qquad (4)$$

where ρ_0 is the normal nuclear density 0.168 fm^{-3}. We have shown [15] that parameters corresponding to a soft equation of state (EOS), $a = -356$ MeV, $b = 303$ MeV, and $\sigma = 7/6$, yield the best fit to experimental data for similar projectile masses and energies. Thus we have utilized a soft EOS exclusively in these calculations. A de-

tailed explanation for the calculation of a residue's excitation energy E^*, spin L, linear momentum $P_\parallel$, etc., has been given elsewhere [15]. For each of the reactions, an ensemble averaged (EA) as well as a single parallel event (SPE) run [15,26,28], which preserves the fluctuations due to nucleon-nucleon collisions, was performed. It was found that the maximum deposited excitation energy predicted by the BUU equation was larger than the total E^* available to the system in the center of mass for each of the SPE interactions. Therefore the excitation energy distributions were adjusted so that the maximum corresponded to the true physical maximum.

Figure 6(a) displays a comparison between the experimental and BUU-PACE mass yield distribution for the interaction of copper with 25 MeV/nucleon ^{22}Ne. Note that the SPE curve provides a better prediction of the experimental data, although it appears to be shifted to lower masses by approximately 7–10 mass units. The slope in the spallation region of the distribution is well represented by the calculation indicating that E^* may be reasonably predicted.

The results for the ^{16}O reaction are shown in Fig. 6(b). Again, the mass yield is better predicted for the SPE run. Although the slope in the exponential region is no longer reproduced, the general shape of the distribution is well represented. The maximum in the distribution is again shifted to smaller masses by 5–7 mass units. Thus, mass yield distribution comparisons suggest that the mass of
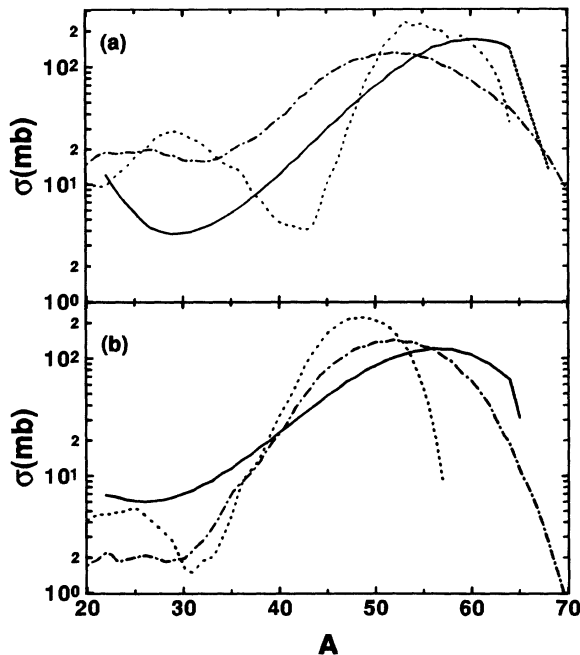
the remnant is underestimated at these energies and in turn results in a poor prediction of the mass yield distribution as compared with the previously published ^{6}Li results [15].

The fractional velocity transfer comparisons for the interaction of copper and 25 MeV/nucleon ^{22}Ne are shown for the EA and SPE calculations in Figs. 7(a) and 7(b), respectively. For the ensemble average, the distribution exhibits a sharp discontinuity at $\Delta A \sim 10$. For $\Delta A < 10$ the calculation predicts nearly complete fractional velocity transfer. The calculated values drop off sharply at this mass loss to values comparable to the experimental data. Between $\Delta A = 10$ and 20 the calculation predicts the experimental distribution well, while for the lightest products the maximum is overpredicted. On the other hand, the SPE fractional velocity transfer predicts a more continuous distribution. Although near-target products are overpredicted, for $\Delta A > 10$ the distribution is well reproduced. It is interesting to note that below $\Delta A = 10$ the calculated distribution increases to a maximum for trans-target products. The experimental data yield similar results. Note that if the calculated distribution were shifted 10 mass units towards the target, the shape of the experimental distribution would be predicted almost exactly, although the absolute magnitude of the calculated values would be larger than the experimental results. This comparison again suggests that the mass of the remnant is underestimated for this reaction.

The results for the ^{16}O fractional velocity transfer comparisons for the ensemble average and single parallel event runs are shown in Figs. 8(a) and 8(b), respectively. The EA calculation appears to better predict the
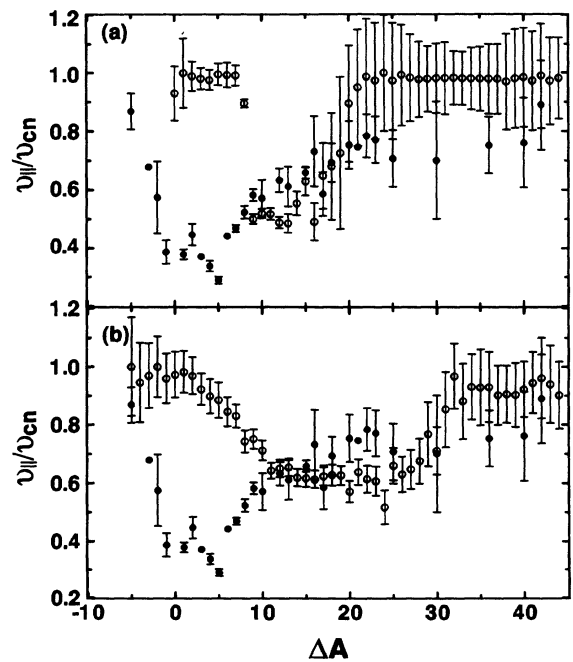

FIG. 6. Comparison of (a) 25 MeV/nucleon ^{22}Ne + Cu experimental mass yield distribution (solid line) with BUU-PACE calculated distribution for ensemble averaged runs (dashed line) and single parallel event runs (dot-dashed line) and (b) 35 MeV/nucleon ^{16}O + Cu experimental mass yield distribution (solid line) with BUU-PACE calculated distribution for ensemble averaged runs (dashed line) and single parallel event runs (dot-dashed line).

FIG. 7. Comparison of the experimental (●) 25 MeV/nucleon ^{22}Ne + Cu fractional velocity transfer with BUU-PACE calculated (o) distributions for (a) an ensemble averaged run and (b) a single parallel event run.
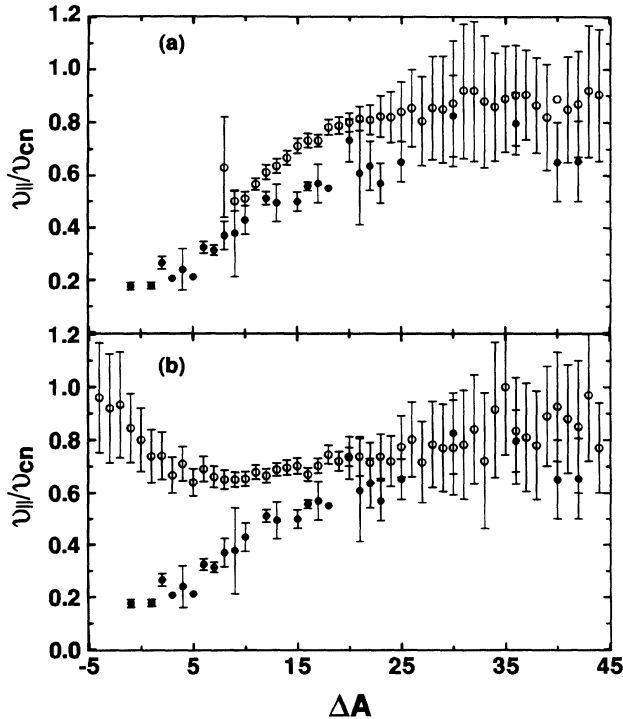
FIG. 8. Comparison of the experimental ($\bullet$) 35 MeV/
nucleon ^{16}O + Cu fractional velocity transfer with BUU-PACE
calculated (o) distributions for (a) an ensemble averaged run
and (b) a single parallel event run.

distribution, although the sharp cutoff in the calculated
mass yield distribution at $A \sim 58$ prevents the compari-
son from being extended to products with $\Delta A < 6$. The
calculated values, where available, are larger than deter-
mined experimentally but the overall shape of the dis-
tribution is well reproduced. The distribution predicted
by the single parallel event run again overpredicts the
values for $\Delta A < 20$. In fact, the calculation predicts
nearly full momentum transfer for near-target and trans-
target products while experimentally these products are
determined to originate in very low momentum transfer
interactions.

It is apparent from the above comparisons that nei-
ther the EA nor the SPE calculation can satisfactorily
reproduce either the mass yield or the velocity transfer
distributions. This is in direct contrast with the com-
parison with 90 MeV/nucleon ^{6}Li data [15], where it was
found that the SPE calculation satisfactorily reproduced
both distributions. It is unclear at present whether this
discrepancy is attributable to the difference in projectile
energy per nucleon or to that in projectile mass.

V. CONCLUSION

The interaction of copper with 25 MeV/nucleon ^{22}Ne,
35 MeV/nucleon ^{16}O, and 40 MeV/nucleon ^{14}N has been

investigated and compared with previously reported re-
sults [14–16] for lighter projectiles at similar total pro-
jectile kinetic energies. The isobaric yields remain es-
sentially unchanged with variation in projectile mass, as
has been shown previously [16]. The ^{16}O and ^{14}N mass
yield distributions also yielded very similar results, where
the maximum in the distributions occurs at $A \sim 55$ and
the minimum at $A \sim 25$–30. On the other hand, ^{22}Ne
exhibits a greater upturn for the lightest products, indi-
cating that binary fragmentation appears more probable
for this heavier projectile. Also, the shift toward larger
masses of the peak in the ^{22}Ne distribution appears to
be a result of the increasing likelihood of complete fusion
with decreasing projectile energy per nucleon and thus
increasing importance of mean field interactions.

The fractional velocity transfer comparisons again re-
veal similar distributions for the ^{16}O and ^{14}N reactions,
while the ^{22}Ne distribution is quite different. First, the
fractional velocity transfer is larger, on average, for the
heavier ion. Second, the distribution for ^{22}Ne exhibits
a V shape centered about the target mass, where the
fractional velocity transfer for trans-target products in-
creases with increasing product mass. Both of these re-
sults appear to be associated with an increase in com-
plete fusion at low energy per nucleon. In fact, when
comparing the results with previously published data, it
is apparent that this V-shaped distribution disappears
above ~ 25 MeV/nucleon, indicating the increasing im-
portance of nucleon-nucleon collisions in governing the
reaction dynamics above this energy. The mean LMT
results show that this quantity increases with projectile
mass at constant projectile energy, a trend that can be
attributed to the concomitant decrease in energy per nu-
cleon. However, light projectiles appear to be more effi-
cient in transferring momentum than the heavier projec-
tiles studied.

Comparisons with BUU-PACE calculations have been
made for the 25 MeV/nucleon ^{22}Ne + Cu and 35
MeV/nucleon ^{16}O + Cu reactions. We have used both
ensemble averaged and single parallel event versions of
BUU. Neither of these versions is able to provide satis-
factory fits to either the mass yield distribution or the
velocity transfer distribution for either projectile. These
results contrast with the satisfactory agreement we pre-
viously obtained with similar data for 90 MeV/nucleon
^{6}Li ions [15].

ACKNOWLEDGMENTS

[1] M. Fatyga et al., Phys. Rev. Lett. 55, 1376 (1985).

[2] V.E. Viola, Nucl. Phys. A471, 53c (1987).

[3] T.C. Awes et al., Phys. Lett. 87B, 48 (1979).

[4] H. Nifenecker et al., Nucl. Phys. A447, 42 (1985).

[5] J. Galin et al., Phys. Rev. Lett. 48, 1787 (1982).

[6] M.B. Tsang et al., Phys. Lett. 134B, 169 (1984).

[7] M. Conjeaud et al., Phys. Lett. 159B, 244 (1985).

[8] G. LaRana et al., Nucl. Phys. A407, 233 (1983).

[9] G. Nebbia et al., Z. Phys. A 311, 247 (1983).

[10] J.L. Laville et al., Phys. Lett. 138B, 25 (1984).

[11] F. Saint-Laurent et al., Phys. Lett. B 202, 190 (1988).

[12] D.X. Jiang et al., Nucl. Phys. A503, 560 (1989).

[13] S.Y. Cho, Y.H. Chung, N.T. Porile, and D.J. Morrissey, Phys. Rev. C 36, 2349 (1987).

[14] S.Y. Cho, N.T. Porile, and D.J. Morrissey, Phys. Rev. C 39, 2227 (1989).

[15] J.P. Whitfield and N.T. Porile, Phys. Rev. C 49, 304 (1994).

[16] J.P. Whitfield and N.T. Porile, Phys. Rev. C 47, 1636 (1993).

[17] L. Pieńkowski, J. Jastrebski, W. Kurcewicz, A. Gizon, J. Blachot, and J. Crancon, Phys. Rev. C 43, 1331 (1991).

[18] T. Lund et al., Phys. Lett. 102B, 239 (1981).

[19] T. Lund et al., Z. Phys. A 306, 43 (1982).

[20] A. Lleres, J. Blachot, J. Crancon, A. Gizon, and H. Nifenecker, Z. Phys. A 312, 177 (1983).

[21] L. Kowalski, P.E. Haustein, and J.B. Cumming, Phys. Rev. Lett. 51, 642 (1983).

[22] W. Loveland, K. Aleklett, L. Sihver, Z. Xu, C. Casey,

and G.T. Seaborg, Nucl. Phys. A471, 1756 (1986).

[23] S. Leray, J. Phys. C 4, 265 (1986).

[24] G.F. Bertsch, H. Kruse, and S. Das Gupta, Phys. Rev. C 29, 673 (1984).

[25] H. Kruse, B.V. Jacak, and H. Stocker, Phys. Rev. C 19, 289 (1985).

[26] G.F. Bertsch and S. Das Gupta, Phys. Rep. 160, 189 (1988).

[27] W. Bauer, G.F. Bertsch, W. Cassing, and U. Mosel, Phys. Rev. C 34, 2127 (1986).

[28] W. Bauer, Nucl. Phys. A471, 604 (1987).

[29] A. Gavron, Phys. Rev. C 21, 230 (1980).

[30] The Stopping and Ranges of Ions in Matter, edited by J.F. Ziegler, J.P. Biersak, and U. Littmark (Pergamon, New York, 1985), Vol. I.

[31] T. Routti and S.G. Prussin, Nucl. Instrum. Methods 72, 125 (1969).

[32] J.B. Cumming, National Academy of Sciences Report No. NAS-NS-3107, 1962 (unpublished), p. 25.

[33] U. Reus and W. Westmeir, At. Data Nucl. Data Tables 29, 2 (1983).

[34] N.T. Porile, G.D. Cole, and C.R. Rudy, Phys. Rev. C 19, 2288 (1979).

[35] G. Rudstam, Z. Naturforsch. 219, 1027 (1966).

[36] L. Winsberg and J.M. Alexander, Phys. Rev. 121, 518 (1961).

[37] J. Hazan and M. Blann, Phys. Rev. 137, B1202 (1965).

[38] W. Bauer, G.F. Bertsch, and S. Das Gupta, Phys. Rev. Lett. 58, 863 (1987).